

Virtual Compton scattering measurements in the nucleon resonance region

A. Blomberg¹, H. Atac¹, N. Sparveris^{1,a}, M. Paolone¹, P. Achenbach², M. Benali³, J. Beričič⁴, R. Böhm², L. Correa², M.O. Distler², A. Esser², D. Flay¹, H. Fonvieille³, I. Friščič², Y. Kohl², H. Merkel², U. Müller², Z.E. Meziani¹, M. Mihovilovic⁴, J. Pochodzalla², A. Polychronopoulou¹, B. Pasquini⁵, M. Schoth², F. Schulz², S. Schlimme², C. Sfienti², S. Sirca^{4,6}, and A. Weber²

¹ Temple University, Philadelphia, PA 19122, USA

² Institut für Kernphysik, Johannes Gutenberg-Universität Mainz, D-55099 Mainz, Germany

³ Clermont Université, Université Blaise Pascal, CNRS/IN2P3, LPC, BP 10448, F-63000 Clermont-Ferrand, France

⁴ Jožef Stefan Institute, SI-1000 Ljubljana, Slovenia

⁵ Dipartimento di Fisica, Università degli Studi di Pavia, I-27100 Pavia, Italy

⁶ Faculty of Mathematics and Physics, University of Ljubljana, SI-1000 Ljubljana, Slovenia

Received: 31 January 2019 / Revised: 11 August 2019

Published online: 22 October 2019

© The Author(s) 2019. This article is published with open access at Springerlink.com

Communicated by N. Kalantar

Abstract. We report on new measurements of the electric Generalized Polarizability (GP) of the proton α_E in a kinematic region where a puzzling dependence on momentum transfer has been observed, and we have found that $\alpha_E = (5.3 \pm 0.6_{stat} \pm 1.3_{sys}) 10^{-4} \text{ fm}^3$ at $Q^2 = 0.20 \text{ (GeV}/c)^2$. The new measurements, when considered along with the rest of the world data, suggest that α_E can be described by either a local plateau or by an enhancement in the region $Q^2 = 0.20 \text{ (GeV}/c)^2$ to $0.33 \text{ (GeV}/c)^2$. The experiment also provides the first measurement of the Coulomb quadrupole amplitude in the $N \rightarrow \Delta$ transition through the exploration of the $p(e, e'p)\gamma$ reaction. The new measurement gives $CMR = (-4.4 \pm 0.8_{stat} \pm 0.6_{sys})\%$ at $Q^2 = 0.20 \text{ (GeV}/c)^2$ and is consistent with the results from the pion electroproduction world data. It has been obtained using a completely different extraction method, and therefore represents a strong validation test of the world data model uncertainties.

1 Introduction

The polarizabilities of a composite system such as the nucleon [1] are fundamental structure constants, just as its size and shape, and can be accessed experimentally by Compton scattering processes. In the case of real Compton scattering (RCS), the incoming real photon deforms the nucleon, and by measuring the energy and angular distributions of the outgoing photon one can determine the global strength of the induced current and magnetization densities, which are characterized by the nucleon polarizabilities. Although the electric, magnetic and some of the spin polarizabilities are known with reasonable accuracy from Compton scattering experiments, little is known about the distribution of polarizability density inside the nucleon. We can gain access to this information through the virtual Compton scattering (VCS) process where the incident real photon is replaced by a virtual photon [2]. The virtuality of the photon allows us to map out the spa-

tial distribution of the polarization densities. In this case it is the momentum of the outgoing real photon q' that defines the size of the perturbation while the momentum of the virtual photon q sets the scale of the observation. In analogy to the form factors for elastic scattering, which describe the charge and magnetization distributions, VCS gives access to the deformation of these distributions under the influence of an electromagnetic field perturbation as a function of the distance scale. The structure dependent part of the process is parametrized by the Generalized Polarizabilities (GPs) which can be seen as Fourier transforms of local polarization densities (electric, magnetic, and spin) [3]. The GPs are therefore a probe of the nucleon dynamics, allowing us, *e.g.*, to study the role of the pion cloud and quark core contributions to the nucleon dynamics at various length scales.

The GPs depend on the quantum numbers of the two electromagnetic transitions involved in the Compton process and typically a multipole notation is adopted. Initially ten independent lowest-order GPs were defined [4]; it was shown [5, 6] that nucleon crossing and charge con-

^a e-mail: sparveris@temple.edu (corresponding author)

jugation symmetry reduce this number to six, two scalar ($S = 0$) and four spin, or vector GPs ($S = 1$). The two scalar GPs, the electric and the magnetic, generalize the well known static electric α_E and magnetic β_M polarizabilities obtained in real Compton scattering [7–10]. Contrary to atomic polarizabilities, which are of the size of the atomic volume, the proton electric polarizability α_E [8] is much smaller than the volume scale of a nucleon (only a few % of its volume). The small size of the polarizabilities reveals the extreme stiffness of the proton as a direct consequence of the strong binding of its inner constituents, the quarks and gluons, while representing a natural indication of the intrinsic relativistic character of the nucleon. In most recent theoretical models the electric GP α_E is predicted to decrease monotonically with Q^2 . The observed smallness of β_M relative to α_E can be explained by the existence of the competing paramagnetic and diamagnetic contributions, which nearly cancel. Furthermore, the β_M polarizability is predicted to go through a maximum before decreasing. This last feature is usually explained by the dominance of diamagnetism due to the pion cloud at long distance, or small Q^2 , and the dominance of paramagnetism due to a quark core at short distance (large Q^2).

VCS is accessed experimentally by exclusive photon electroproduction. The main kinematic variables are the CM 3-momenta \vec{q}_{cm} and \vec{q}'_{cm} of the initial and final photons respectively, the CM angles of the outgoing real photon w.r.t. \vec{q}_{cm} : the polar angle $\theta_{\gamma^*\gamma}$ and the azimuthal angle ϕ , and the 4-momentum transfer squared Q^2 . The photon electroproduction amplitude can be decomposed into the Bethe-Heitler (BH), the Born, and the non-Born contributions. The BH and VCS Born parts are well known and entirely calculable with the nucleon electromagnetic (EM) form factors as inputs, while the non-Born part involves the structure dependent component, parametrized by the GPs. In order to extract the GPs from measurements of photon electroproduction cross sections one can utilize two methods. The first method involves the Low Energy Theorem (LET) [4] and is valid below pion threshold only. The second method involves the Dispersion Relations (DR) approach [11–13] and its domain of validity includes the $\Delta(1232)$ resonance up to the $N\pi\pi$ threshold. When the VCS reaction is measured in the $\Delta(1232)$ resonance region the VCS non-Born part offers access to additional information, such as the $N \rightarrow \Delta$ transition form factors [14]. An extensive experimental and theoretical effort has focused on this subject in the past two decades. Particular attention has been addressed to the two quadrupole transition amplitudes, the Electric and the Coulomb, which offer a path for the exploration of the non-spherical components in the nucleon wavefunction. A review of this topic is presented in [15].

2 The experimental measurements

The measurements were performed at $Q^2 = 0.20$ (GeV/c)² and in the $\Delta(1232)$ resonance region. The experiment aims to study the electric Generalized Polarizability of the proton α_E in a region where two MAMI experiments [16, 17] have identified an unexpected enhancement

of α_E , at $Q^2 = 0.33$ (GeV/c)², that can not be accommodated along with the other experimental measurements at different Q^2 with a single dipole fall-off in Q^2 . In this work an additional opportunity is also presented to access for the first time the $N \rightarrow \Delta$ quadrupole amplitudes through the measurement of the photon channel and to offer a valuable cross check to the world data. The two quadrupole transition amplitudes have so far been explored only through pion electroproduction measurements. In this work we have explored the Coulomb quadrupole for the first time through the VCS reaction, providing a measurement through a different reaction mechanism and within a completely different theoretical framework.

The experiment kinematics focused on $\theta_{\gamma^*\gamma} > 120^\circ$ in order to avoid the kinematic region where the BH process dominates and to allow for the sensitivity to the measured signal to be maximal. The VCS cross section was measured, as well as the in-plane azimuthal asymmetry of the VCS cross section with respect to the momentum transfer direction

$$A_{(\phi_{\gamma^*\gamma}=0,\pi)} = \frac{\sigma_{\phi_{\gamma^*\gamma}=0} - \sigma_{\phi_{\gamma^*\gamma}=180}}{\sigma_{\phi_{\gamma^*\gamma}=0} + \sigma_{\phi_{\gamma^*\gamma}=180}}.$$

The asymmetry allows for part of the cross section's systematic uncertainties to be suppressed thus improving the precision of the measurements and amplifying the sensitivity to the measured amplitudes.

The experiment utilized the A1 spectrometer setup at MAMI [18]. A 1.1 GeV unpolarized electron beam with a beam current of 20 μ A was employed on a 5 cm liquid hydrogen target, while the beam was rastered across the target to avoid boiling. The recoil proton and the scattered electron were detected in coincidence with spectrometers A and B [18], while the undetected photon of the VCS reaction was identified through the missing mass spectrum. Each spectrometer contains two vertical drift chambers, two scintillator planes, and a Cherenkov detector, while both spectrometers offer a momentum resolution of 10^{-4} . The experimental setup offered a better than 1 ns (FWFM) resolution in the coincidence timing spectrum, while the subtraction of the random coincidences introduced a minor uncertainty as a result of the small contribution of the random coincidences under the coincidence timing peak and of the excellent timing resolution. The photon electroproduction events were further identified through the missing-mass reconstruction as shown in fig. 1 (right panel), where one can clearly observe the photon peak as well as the π^0 -electroproduction peak which also falls within the spectrometer acceptance, with the two peaks being very well separated. An extensive description of the experimental arrangement and parameters, as well as of the data analysis can be found in [19, 20].

A calibration was performed to the central momenta of the two spectrometers by simultaneously optimizing the experimental missing mass peak position and width. An additional constraint in determining the actual momentum settings of both spectrometers is offered by the fact that in the asymmetry measurements the electron spec-

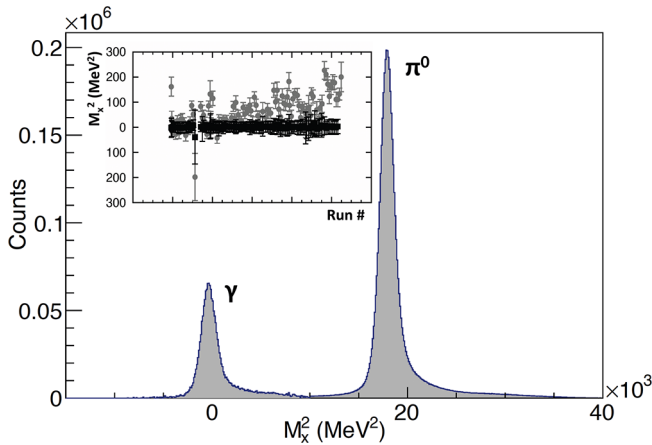


Fig. 1. The missing mass spectrum. The two peaks corresponding to the photon and to the π^0 are very well separated. The photon peak has been multiplied by a factor of 10 so that it can be clearly seen in the figure. The inserted panel shows the center of the photon missing mass peak before (gray circle) and after (black box) the momentum calibration as a function of the different run numbers.

trometer settings as well as the proton spectrometer momentum remain fixed [19]. The calibration resulted in a 0.4% correction to the proton spectrometer momentum and in a 0.1% to the electron spectrometer one. Furthermore, an observed ice-build up at the target that affected the missing mass reconstruction was studied and corrected for in the analysis. In fig. 1 (right panel insert) one can see the center of the photon missing mass as a function of the different run numbers.

In order to determine the experimental cross section the five-fold solid angle is calculated through a Monte Carlo simulation that offers an accurate description of the experimental setup, including the intrinsic resolution of the detectors and energy losses. The radiative corrections have been included in the simulation and they are accounted for as described in [21]. In order to extract the experimental cross section the generated events in the simulation are weighted with a cross section using the DR calculation of [11, 12]. The calculation includes the BH+Born and the non-Born contributions, where one can utilize different parameterizations for the non-Born part. For the non-Born part a realistic initial parametrization is applied based on the current knowledge of the GPs as well as that of the $N \rightarrow \Delta$ transition amplitudes, the experimental cross sections are determined, and the scalar GPs are then set as free parameters and are extracted utilizing the DR framework [19, 22]. Then the process is repeated by using the extracted parameters as a new input in the simulation cross section, and the amplitudes of interest are then extracted again. This procedure converges quickly and the extracted values for the GPs are at that point finalized. If the procedure is repeated by utilizing a different initial parametrization for the non-Born part the converging results are independent of the initial input parameters.

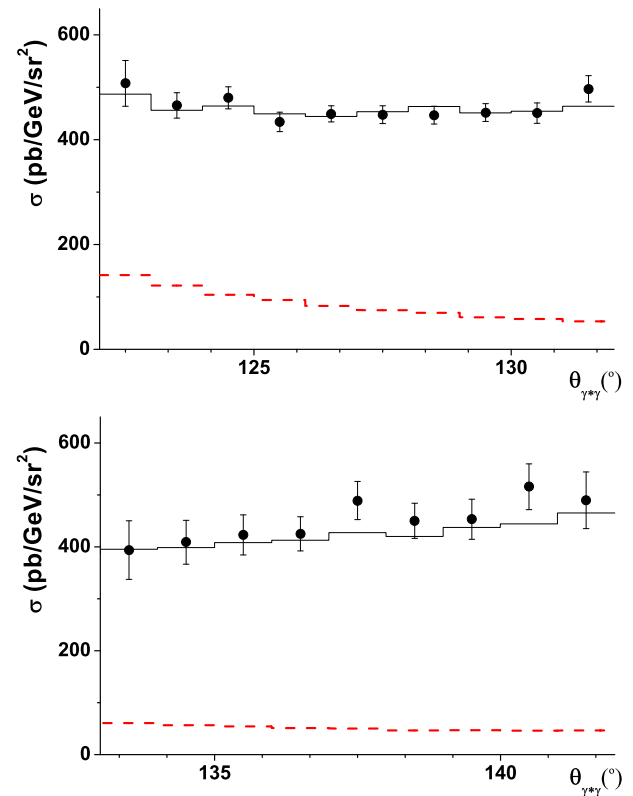


Fig. 2. Experimental cross sections as a function of the spectrometer acceptance at $\phi_{\gamma^*\gamma} = 0^\circ$. The BH+Born contribution (dashed line) is compared to the DR calculation for the total cross section (solid line).

The BH+Born contribution accounts for $\approx 20\%$ of the total cross section (see fig. 2) for all experimental settings. The primary sources of systematic uncertainties involve the uncertainties in the momenta and the angles of the two spectrometers, the luminosity, the knowledge of the acceptance, and the radiative corrections. For the spectrometer momenta the effect of an uncertainty of $\pm 2 \cdot 10^{-4}$ was studied by varying the momentum settings accordingly, repeating the analysis process, and the deviation of the extracted results was quantified as the corresponding uncertainty. A similar procedure was also followed to study the effect of the uncertainty in the spectrometer angles, where the variation involved was ± 0.1 mr for each one of the two spectrometers. The effect of these uncertainties varies among the settings but is in principle of the order of $\pm 1\%$. The uncertainty to the solid angle, the luminosity, and the radiative corrections added quadratically is $\approx \pm 2.5\%$. The statistical uncertainty on the cross section is typically smaller, ranging between 1.5% and 2%.

For the electric Generalized Polarizability the extracted value is $\alpha_E = (5.3 \pm 0.6 \pm 1.3) \cdot 10^{-4} \text{ fm}^3$ at $Q^2 = 0.20 \text{ (GeV/c)}^2$, where the first uncertainty is statistical and the second is the systematic one. The magnetic GP was also treated as a free parameter in the analysis but was constrained within a very large uncertainty, something to be expected since the experiment kinematics were

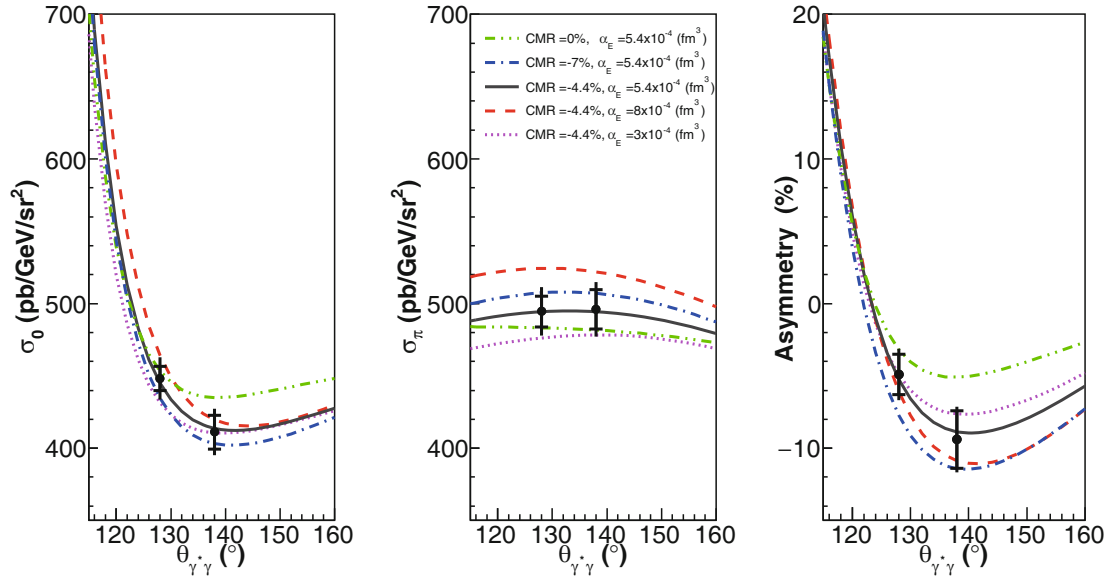


Fig. 3. Cross sections and asymmetries measured at $Q^2 = 0.20$ (GeV/c)². The solid line corresponds to the DR calculation with the extracted values for α_E and for CMR . The dashed and the dotted curves show the effect from a variation to the central value of α_E , from $3 \cdot 10^{-4} \text{ fm}^3$ to $8 \cdot 10^{-4} \text{ fm}^3$, while the dash-dot-dot and the dash-dot curves show the effect from the variation to the CMR value, from 0% to -7% .

optimized for the measurement of α_E . The spin dependent part of the GPs has been accounted for in the analysis through the predictions of the DR calculation, as typically done in all similar measurements in the past. The effect of using different parameterizations for the proton form factors in the analysis was explored since these quantities enter the calculation of the BH+Born cross section. A systematic study was performed by applying different parameterizations in the analysis, and the variation of the α_E results was determined to be $\pm 0.3 \cdot 10^{-4} \text{ fm}^3$. An uncertainty of $\pm 0.4 \cdot 10^{-4} \text{ fm}^3$ is associated with the uncertainty of the resonant dipole and quadrupole amplitudes. These values were treated as systematic uncertainties and were integrated into the overall systematic uncertainty.

The experimental measurements offer sensitivity to the $N \rightarrow \Delta$ transition Coulomb quadrupole amplitude, which is typically quantified through the CMR ratio to the dominant magnetic dipole amplitude. The Coulomb quadrupole has been previously measured at the same Q^2 through the $p(\vec{e}, e'p)\pi^0$ reaction, utilizing the same experimental setup as in this work, giving the result $CMR = (-5.09 \pm 0.28_{stat+sys} \pm 0.30_{mod})\%$ [23]. If this amplitude is set as a free parameter in the analysis of the VCS measurements we derive the value of $CMR = (-4.4 \pm 0.8_{stat} \pm 0.6_{sys})\%$, which is in very good agreement with the result derived from the pion channel measurement [23]. In this case the central value for the electric GP increases slightly to $\alpha_E = 5.4 \cdot 10^{-4} \text{ fm}^3$. In fig. 3 the measured cross sections and asymmetries for a fixed $Q^2 = 0.20$ (GeV/c)² are presented. The solid line corresponds to the DR calculation with the extracted values for α_E and CMR as an input. The dashed and the dotted lines exhibit the effect from the variation of α_E , while the dash-dot and the dash-dot-dot lines show the effect of a variation on the CMR .

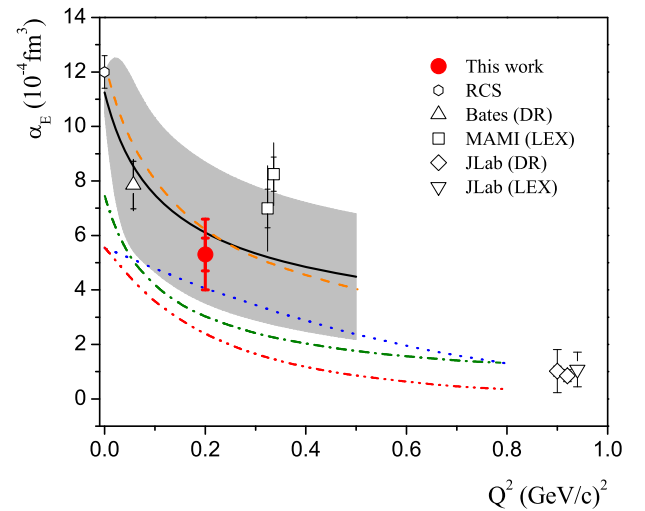


Fig. 4. The world data on the electric GP, with statistical (inner) and total error bar. The result from this work (solid circle) as well as the measurements from Bates [24], MAMI [16, 17, 25], JLab [26, 22] and the RCS [8] are shown. The theoretical calculations BChPT [27] (solid line with uncertainty band), HBChPT [28] (dash), NRQCM [29] (dot), Effective Lagrangian Model [30] (dash-dot-dot) and Linear Sigma Model [31] (dash-dot) are also shown.

3 Discussion and conclusions

In this experiment we have performed a measurement of α_E in a kinematic region where a puzzling dependence on the momentum transfer has been observed. The result for the electric GP is shown in fig. 4, along with the world data from Bates [24], MAMI [16, 17], JLab [26, 22] and the RCS [8]. The new result suggests that α_E follows a fall-

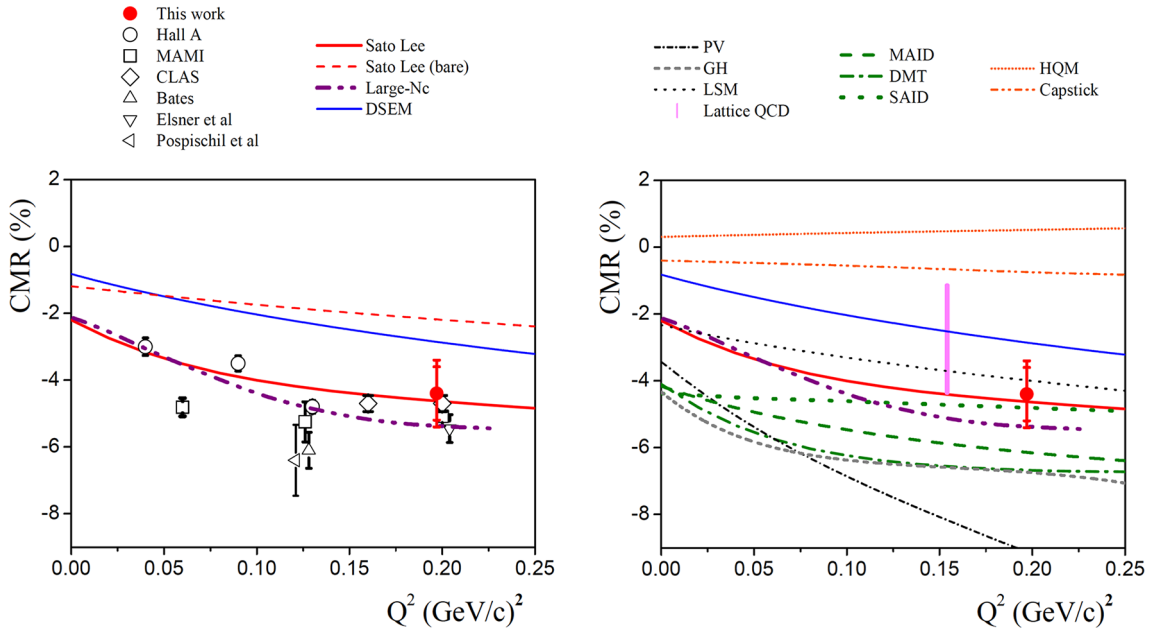


Fig. 5. Left panel: the CMR measurement from this work (solid circle) and from [23,33–39] (open symbols) are presented. All data points are shown with their total experimental uncertainties (statistical and systematic) added in quadrature. The theoretical predictions of Sato-Lee [40] (full and bare), the large- N_c calculation [41], and the DSEM [42] are also shown. Right panel: the CMR measurement from this work (solid circle) is shown along with all the available theoretical calculations: MAID [43,44], DMT [45], SAID [46–48], Sato-Lee [40], Capstick [49], HQM [50], the Lattice-QCD calculation [51], the large- N_c calculation [41], the DSEM [42], the linear σ -model (LSM) [52], the ChEFT of Pascalutsa-Vanderhaegen (PV) [53] and the Gail-Hemmert (GH) [54].

off with Q^2 after the Bates data point [24] at $Q^2 = 0.06$ (GeV/c)². Then α_E can be described by either an enhancement, or by a local plateau, in the range of $Q^2 = 0.20$ (GeV/c)² to 0.33 (GeV/c)², before it then continues with a more drastic fall-off towards the JLab measurement at $Q^2 = 0.9$ (GeV/c)². A dipole fall off of α_E that has been suggested by the Bates [24] and the JLab [26,22] data, but not supported by the MAMI [16,17] ones, is consistent only with the lower end of the α_E experimental uncertainty of our results at 0.20 (GeV/c)². Another MAMI experiment [32] has performed measurements of the electric GP in the same momentum transfer region and its upcoming results are expected to shed more light into the Q^2 dependence of α_E . The α_E polarizability has been studied within a variety of theoretical frameworks, as exhibited in fig. 4, and the new measurement offers new input, and constraints, to these calculations. Our results are in agreement with the NLO HBChPT [28] calculation that includes the Delta isobar in the ϵ -expansion. The NLO BChPT calculation with Delta degrees of freedom by [27] has a relatively large uncertainty (shown by the blue band) and can not discriminate between the results of the new and previous MAMI experiments. The predictions of the NRQCM [29], Effective Lagrangian Model [30], and the Linear Sigma Model [31] tend to underestimate the magnitude of α_E , as also suggested by the rest of the world data. It has to be pointed out that all theoretical calculations predict a monotonic fall off of α_E and none of them

is able to account for a non trivial Q^2 dependence that the world data suggest.

An extraction of the CMR has been performed for the first time through the measurement of the $p(e, e'p)\gamma$ reaction. The new result is presented in fig. 5 (left panel), along with the results from the pion channel measurements [23, 33–39]. One can note the excellent agreement between the photon and the pion channel results at $Q^2 = 0.20$ (GeV/c)². The data are compared to the theoretical predictions of Sato-Lee [40] (full and bare), the DSEM [42], and the linear σ -model (LSM) [52]. One can note that the Sato Lee prediction has a remarkable success in describing the Q^2 evolution of the Coulomb quadrupole amplitude, providing a strong support to the interpretation within the model that the Δ resonance consists of a bare quark-gluon core and a pion cloud, and the large pion cloud contribution to CMR can be seen by comparing the Sato Lee “full” and “bare” curves. One can further observe that the dashed curve of the Sato Lee “bare” component is qualitatively similar to the prediction of a model based on the Dyson-Schwinger Equation of QCD [42] (DSEM) which does not include the pion degree of freedom, and thus the agreement between the data and the Sato Lee prediction suggests a possible link between the bare quark-core of a dynamical model and the genuine QCD dynamics. In fig. 5 (right panel) the results are compared to all available theoretical calculations: the phenomenological analysis of MAID [43,44], DMT [45], SAID [46–48] and the

theoretical predictions of Sato-Lee [40], Capstick [49], hypercentral quark model (HQM) [50], the Lattice-QCD calculation [51], the large- N_c calculation [41], the DSEM [42], the linear σ -model (LSM) [52], the chiral effective field theory of Pascalutsa-Vanderhaegen (PV) [53] and the Gail-Hemmert (GH) [54]. The results support the dominant role of the mesonic degrees of freedom at the large distance scale and the conclusion that approximately half of the magnitude of the Coulomb quadrupole amplitude is attributed to the mesonic cloud at low Q^2 , as also suggested by the pion channel measurements [23]. The unique aspect of this measurement is that it is the first measurement performed through a different reaction channel and utilizes a completely different extraction framework. This is an important step considering that the world data for the resonant quadrupole amplitudes are typically accompanied by a model uncertainty that is associated with the treatment of the numerous physical background amplitudes and is not sufficiently constrained through the experimental measurements of the pion channel. A theoretical model is typically utilized for the treatment of these amplitudes thus introducing a model uncertainty to the world data results. A future re-analysis of the same data, utilizing a new theoretical model, could thus potentially increase the significance of these model uncertainties. In this work, we explored the same quantity through a different reaction mechanism and within a completely different theoretical framework, thus providing a cross-check of the results for the CMR extracted via pion electroproduction as well as an independent verification of the world data model uncertainties

We would like to thank the MAMI accelerator staff for their outstanding support. This work is supported by the US Department of Energy award DE-SC0016577, by the Federal State of Rhineland-Palatinate, and by the German Research Foundation with the Collaborative Research Center 1044.

Data Availability Statement This manuscript has no associated data or the data will not be deposited. [Authors' comment: The data related to this publication, in their raw and filtered format, are stored in data disks currently at the Temple University Physics Department and they are available upon request. The data related to this publication are further described in the thesis of A. Blomberg (A. Blomberg, PhD Thesis, Temple University (2016)).]

Publisher's Note The EPJ Publishers remain neutral with regard to jurisdictional claims in published maps and institutional affiliations.

Open Access This is an open access article distributed under the terms of the Creative Commons Attribution License (<http://creativecommons.org/licenses/by/4.0>), which permits unrestricted use, distribution, and reproduction in any medium, provided the original work is properly cited.

References

1. F. Hagelstein, R. Miskimen, V. Pascalutsa, *Prog. Part. Nucl. Phys.* **88**, 29 (2016).
2. P.A.M. Guichon, M. Vanderhaeghen, *Prog. Part. Nucl. Phys.* **41**, 125 (1998).
3. M. Gorchtein, C. Lorce, B. Pasquini, M. Vanderhaeghen, *Phys. Rev. Lett.* **104**, 112001 (2010).
4. P.A.M. Guichon, G.Q. Liu, A.W. Thomas, *Nucl. Phys. A* **591**, 606 (1995).
5. D. Drechsel, G. Knochlein, A.Y. Korchin, A. Metz, S. Scherer, *Phys. Rev. C* **57**, 941 (1998).
6. D. Drechsel, G. Knochlein, A.Y. Korchin, A. Metz, S. Scherer, *Phys. Rev. C* **58**, 1751 (1998).
7. V. Olmos de Leon *et al.*, *Eur. Phys. J. A* **10**, 207 (2001).
8. M. Schumacher, *Prog. Part. Nucl. Phys.* **55**, 567 (2005).
9. M. Schumacher, M.D. Scadron, *Fortsch. Phys.* **61**, 703 (2013).
10. B. Pasquini, P. Pedroni, S. Sconfiatti, arXiv:1903.07952.
11. B. Pasquini, M. Gorchtein, D. Drechsel, A. Metz, M. Vanderhaeghen, *Eur. Phys. J. A* **11**, 185 (2001).
12. D. Drechsel, B. Pasquini, M. Vanderhaeghen, *Phys. Rep.* **378**, 99 (2003).
13. B. Pasquini, M. Vanderhaeghen, *Annu. Rev. Nucl. Part. Sci.* **68**, 75 (2018).
14. N. Sparveris *et al.*, *Phys. Rev. C* **78**, 018201 (2008).
15. A.M. Bernstein, C.N. Papanicolas, *AIP Conf. Proc.* **904**, 1 (2007).
16. J. Roche *et al.*, *Phys. Rev. Lett.* **85**, 708 (2000).
17. P. Janssens *et al.*, *Eur. Phys. J. A* **37**, 1 (2008).
18. K.I. Blomqvist *et al.*, *Nucl. Instrum. Methods A* **403**, 263 (1998).
19. A. Blomberg, PhD Thesis, Temple University (2016).
20. N. Sparveris *et al.*, *Study of the nucleon structure by Virtual Compton Scattering measurements at the Δ resonance*, MAMI A1 Proposal.
21. M. Vanderhaeghen *et al.*, *Phys. Rev. C* **62**, 025501 (2000).
22. H. Fonvieille *et al.*, *Phys. Rev. C* **86**, 015210 (2012).
23. N.F. Sparveris *et al.*, *Phys. Lett. B* **651**, 102 (2007).
24. P. Bourgeois *et al.*, *Phys. Rev. Lett.* **97**, 212001 (2006).
25. H. Fonvieille, *Prog. Part. Nucl. Phys.* **55**, 198 (2005).
26. G. Laveissiere *et al.*, *Phys. Rev. Lett.* **93**, 122001 (2004).
27. V. Lensky, V. Pascalutsa, M. Vanderhaeghen, *Eur. Phys. J. C* **77**, 119 (2017).
28. T.R. Hemmert, B.R. Holstein, G. Knochlein, D. Drechsel, *Phys. Rev. D* **62**, 014013 (2000).
29. B. Pasquini, S. Scherer, D. Drechsel, *Phys. Rev. C* **63**, 025205 (2001).
30. A. Korchin, O. Scholten, *Phys. Rev. C* **58**, 1098 (1998).
31. A. Metz, D. Drechsel, *Z. Phys. A* **356**, 351 (1996).
32. H. Merkel *et al.*, MAMI-A1 proposal A1-1/09 (2009), <http://www1.kph.uni-mainz.de/A1/publications/proposals/MAMI-A1-1-09.pdf>.
33. T. Pospischil *et al.*, *Phys. Rev. Lett.* **86**, 2959 (2001).
34. N.F. Sparveris *et al.*, *Phys. Rev. Lett.* **94**, 022003 (2005).
35. S. Stave *et al.*, *Eur. Phys. J. A* **30**, 471 (2006).
36. D. Elsner *et al.*, *Eur. Phys. J. A* **27**, 91 (2006).
37. I.G. Aznauryan *et al.*, *Phys. Rev. C* **80**, 055203 (2009).
38. A. Blomberg *et al.*, *Phys. Lett. B* **760**, 267 (2016).
39. N. Sparveris *et al.*, *Eur. Phys. J. A* **49**, 136 (2013).
40. T. Sato, T.-S.H. Lee, *Phys. Rev. C* **63**, 055201 (2001).

41. V. Pascalutsa, M. Vanderhaeghen, Phys. Rev. D **76**, 111501 (2007).
42. Jorge Segovia, Ian C. Clot, Craig D. Roberts, Sebastian M. Schmidt, Few Body Syst. **55**, 1185 (2014).
43. S.S. Kamalov *et al.*, Phys. Lett. B **522**, 27 (2001).
44. D. Drechsel *et al.*, Nucl. Phys. A **645**, 145 (1999).
45. S.S. Kamalov, S.N. Yang, Phys. Rev. Lett. **83**, 4494 (1999).
46. R.A. Arndt *et al.*, Phys. Rev. C **66**, 055213 (2002).
47. R.A. Arndt *et al.*, Phys. Rev. C **66**, 055213 (2002). arXiv:nucl-th/0301068.
48. R.A. Arndt *et al.*, Phys. Rev. C **66**, 055213 (2002). <http://gwdac.phys.gwu.edu>.
49. S. Capstick, G. Karl, Phys. Rev. D **41**, 2767 (1990).
50. M. De Sanctis *et al.*, Nucl. Phys. A **755**, 294 (2005).
51. C. Alexandrou *et al.*, Phys. Rev. Lett. **94**, 021601 (2005).
52. M. Fiolhais, B. Golli, S. Sirca, Phys. Lett. B **373**, 229 (1996).
53. V. Pascalutsa, M. Vanderhaeghen, Phys. Rev. D **73**, 034003 (2006).
54. T.A. Gail, T.R. Hemmert, Eur. Phys. J. A **28**, 91 (2006).